JMEPEG (2010) 19:1071–1089
DOI: 10.1007/s11665-010-9598-0

1059-9495/$19.00

A Review of FSW Research on Dissimilar Metal and Alloy Systems

L.E. Murr

(Submitted December 9, 2009)

This review summarizes friction-stir welding (FSW) research over a period of a decade and a half, involving 18 different same materials FSW reference systems, and the FSW of 25 different, dissimilar materials systems. These are summarized in tables. The FSW of dissimilar materials systems is distinguished from same materials systems FSW by the formation of complex, intercalated vortex, and related flow patterns. These intercalated, lamellar-like patterns represent solid-state flow by dynamic recrystallization (DRX) which facilitates unrecrystallized, block flow in the DRX regime. A detailed characterization of representative systems involving optical and transmission electron microscopy is also presented. Residual microindentation hardness or other hardness measured across the weld face provides comparative performance signatures for the same material FSW systems in contrast to the dissimilar FSW systems. Hardness fluctuations or complex spikes occurring in the dissimilar systems are skewed from the weld centerline and are shifted when the tool rotation direction changes or the advancing side is reversed.

Keywords dissimilar materials FSW, dynamic recrystallization, flow patterns, optical metallography, TEM

1. Introduction and Overview

After two decades of development, friction-stir welding (FSW) has become a viable and important manufacturing alternative or fabrication component, especially in aerospace or aeronautics applications involving aluminum alloys (Ref 1-5). While FSW began as a joining alternative for aluminum alloys, it has now progressed to higher temperature systems including stainless steels, titanium, and titanium alloys (Ref 6-8). Interest has also mounted for FSW of dissimilar metals and alloys, particularly systems which are difficult or impossible to weld by conventional, thermal (or fusion) welding. FSW has also been demonstrated to be extremely effective in joining aluminum metal matrix composites (MMCs) such as Al (6061) + 20% Al_2O_3 and aluminum alloy A339 containing 20% SiC, as well as MMC's welded to other dissimilar aluminum alloys (Ref 9-11), and aluminum alloys welded to magnesium alloys by FSW (Ref 12-14).

In contrast to conventional, fusion welding, FSW does not involve melt. The joining of similar or dissimilar metals and alloys in FSW is achieved by extreme deformation creating dynamic recrystallization (DRX) which permits flow in the solid-state by sliding between reccrystallized, equiaxed, and usually submicron grains in the weld zone (Ref 12-17). Figure 1(a) shows the FSW process in a simple sequence of schematic views while Fig. 1(b) illustrates the microstructure evolution associated with deformation in the FSW zone leading to DRX. In these schematic views, the head pin (HP) or pin tool is rotated clockwise (cw) at some speed R (rotations/min: rpm) while the tool is advanced at some traverse speed (T) in units of mm/s. In the schematic arrangement shown in Fig. 1(a), the two plates to be welded are labeled A and B, with A representing the advancing side of the weld for the pin tool rotating clockwise (cw). However, when the pin tool rotates counter-clockwise (ccw), B becomes the advancing side of the weld while A is referred to as the trailing or retreating side. The advancing side of the weld is stirred into the retreating side, and as illustrated schematically in Fig. 1(b), it is not necessary for complete recrystallization to occur in both A and B in order to affect solid-state flow and mixing. Indeed, blocks or intercalated segments can flow in the DRX regime just as segments of solid matter flow in a liquid matrix. Material is often deformed in thin strips which are intercalated with softer DRX material forming vortex and related flow features within the weld zone. These intercalated features can occur in the FSW of the same material (A = B in Fig. 1a) while they are exaggerated in dissimilar welds (A ≠ B in Fig. 1a). These features are illustrated in Fig. 1(c) and (d) involving the FSW of aluminum alloy 2024 on the left and silver on the right; with the pin tool rotating clockwise, in Fig. 1(c). The weld zone for the FSW of butted plates in Fig. 1(c) is shown in Fig. 1(d) where the intercalation of Al 2024 and Ag is observed. The dark Al 2024 bands in Fig. 1(d) are the DRX flow zones while the Ag bands are observed to be largely unaltered from the starting plate (Fig. 1c).

It should be noted in Fig. 1a that the pin tool holder (or chuck shoulder) is involved in the FSW process and the FSW structure in the top surface (perpendicular to the z-axis in Fig. 1a at 5) is different from that in the face of the weld zone as shown in the weld plane (in 4), which is perpendicular to the x-axis. The initial view of the butted plates in Fig. 1(c) represents the "surface plane" while, as noted, the FSW structure shown in Fig. 1(d) represents the "weld plane" or weld face plane.

L.E. Murr, Department of Metallurgical and Materials Engineering, The University of Texas at El Paso, El Paso, TX 79968. Contact e-mail: lemurr@utep.edu.

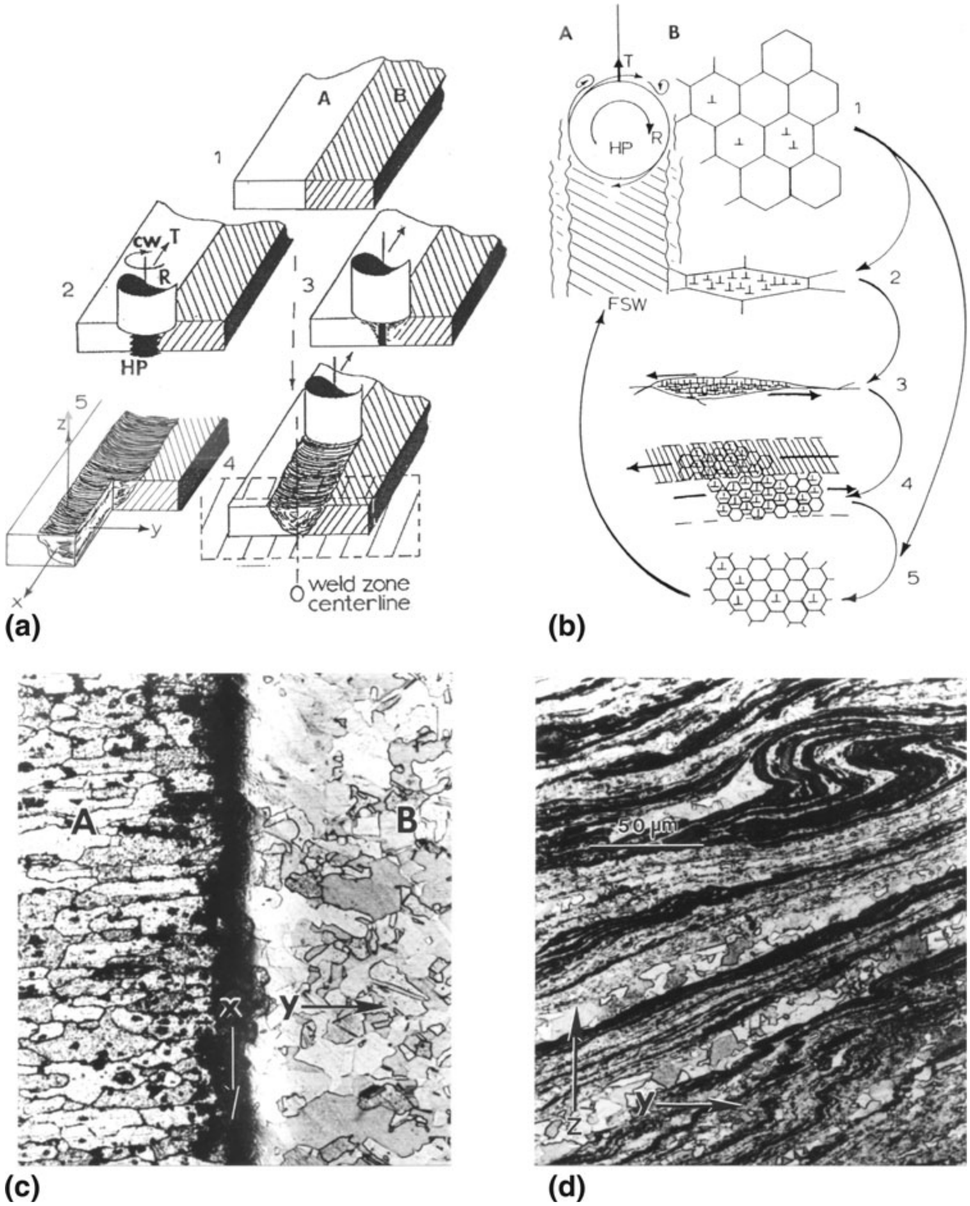

Fig. 1 (a) Schematic sequence (1-5) illustrating the FSW process and conventions: clockwise (cw) rotation (*R*) and head pin (HP) or tool traverse (*T*) along the butted base plates (A and B). In normal operation, the tool is stationary and the base plates (on a backing plate) move into the rotating tool. Numbers 4 and 5 show the weld face plane perpendicular to the *x*-axis and the weld surface (plane) which is perpendicular to the *z*-axis. (b) Schematic illustrating prominent microstructure development in the weld zone. 1 shows the original grain structure for the base plates. In 2, the grains are deformed (distorted) and dislocation density increases. 3 is a precursor to dynamic recrystallization (DRX) in 4. 5 illustrates grain growth after DRX. (c) Optical metallographic view for butted plates of Al 2024 at A and Ag at B viewed along the *z*-axis (5 in a). Weld zone region for FSW of (c) showing complex, intercalated solid-state flow. (a) is after Ref 16. (b) is after Ref 17

Figure 2(a) illustrates the weld plane view for the FSW of columnar grained 1100 aluminum (Ref 18). This example illustrates a large columnar grain structure in the base plates prior to welding in contrast to the weld zone which in Fig. 2(a) contains DRX grains which are far too small to resolve in the optical metallographic image. In contrast to Fig. 2(a), Fig. 2(b) and (c) illustrates the base structure for Al 2024 prior to FSW and the weld zone following FSW, showing smaller, equiaxed DRX grains which have grown by residual heating. Benavides et al. (Ref 19, 20) have shown that in Al 2024 FSW at temperatures as low as −100 °C (under liquid nitrogen) the grain size was near the so-called steady-state grain size or the incipient DRX grain size: roughly 0.7 µm as shown in Fig. 2(d) and (e) in contrast to the weld zone grain size of ~1.5 µm illustrated in Fig. 2(c). Figure 2(e) shows a transmission electron microscope view of the grain structure in Fig. 2(d). Figure 3 shows the corresponding Vickers microindentation hardness (VHN: Vickers Hardness Number) profiles through the weld face center (equi-distant from the top and bottom of the welded plates as shown at 4 in Fig. 1(a) at −100 °C and room temperature. Figure 3 illustrates a standard protocol for assessing the characteristics of an FSW zone in contrast to the

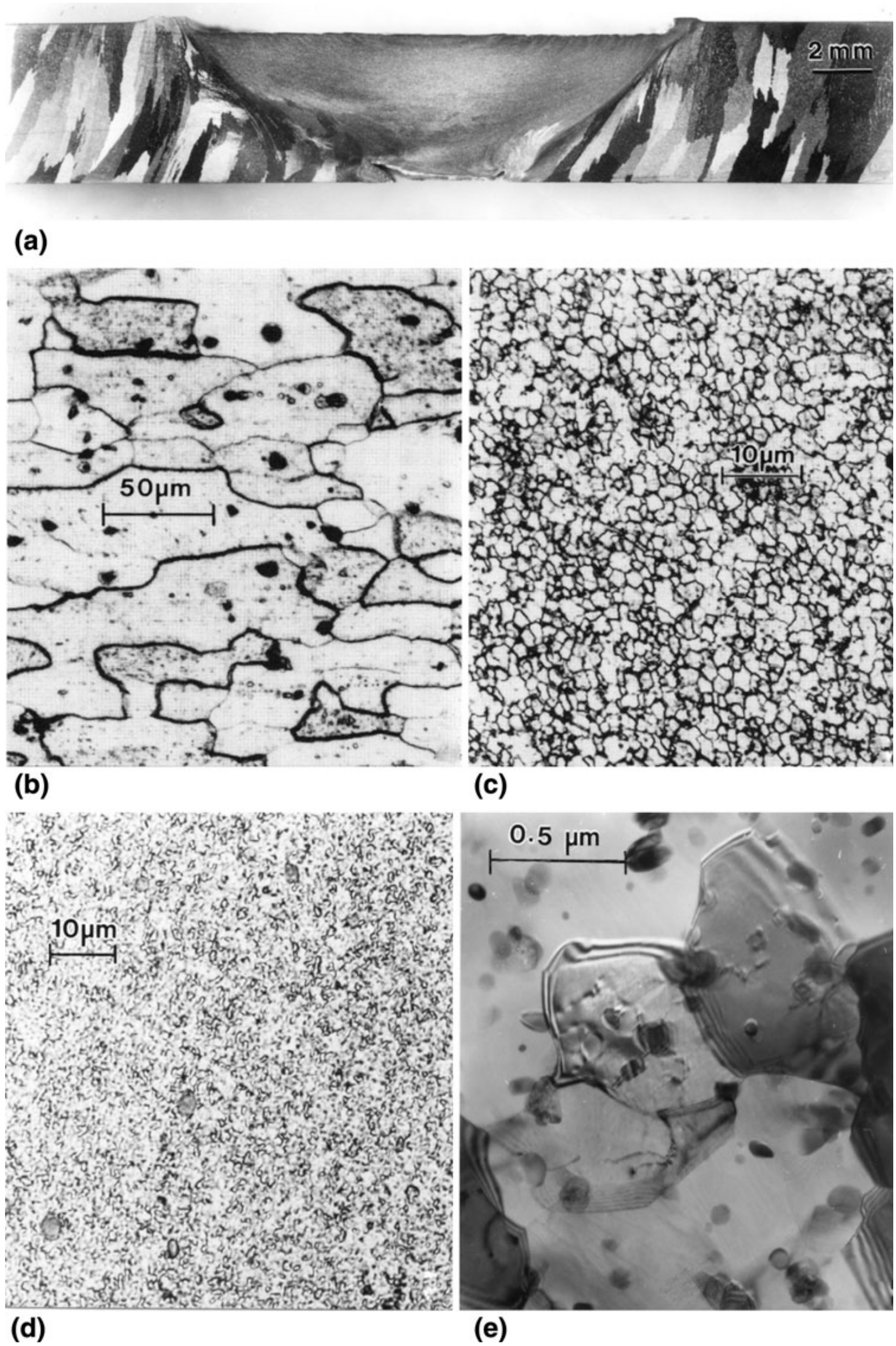

Fig. 2 (a) Friction-stir welded, columnar grained aluminum 1100 alloy (R = 400 rpm, T = 1 mm/s); from Ref 18. (b) Al 2024 unwelded base plate. (c) Weld zone center after FSW of (b) at 800 rpm and 1 mm/s tool traverse speed. (d) Weld zone center for Al 2024 following FSW under liquid nitrogen to achieve a nominal temperature of −100 °C. (e) TEM view of grain structure in (d)

unwelded base material. It can be noted that the weld zone hardness drops considerably and the weld zone edges are the softest. Figure 3 also illustrates the so-called heat-affected zone (HAZ) in contrast to the stir-affected zone (SAZ), also referred to as the thermomechanically affected zone (TMAZ), which includes the weld zone and the transition from the weld zone and the deformed base material. The decline in hardness shown in Fig. 3 results from the softening of the DRX material in the weld zone, the aging characteristics of Al 2024, and corresponding microstructure (especially precipitation) changes.

In contrast to the softening in the weld zone shown in Fig. 3 and the extent of the HAZ in Al 2024, some FSW systems

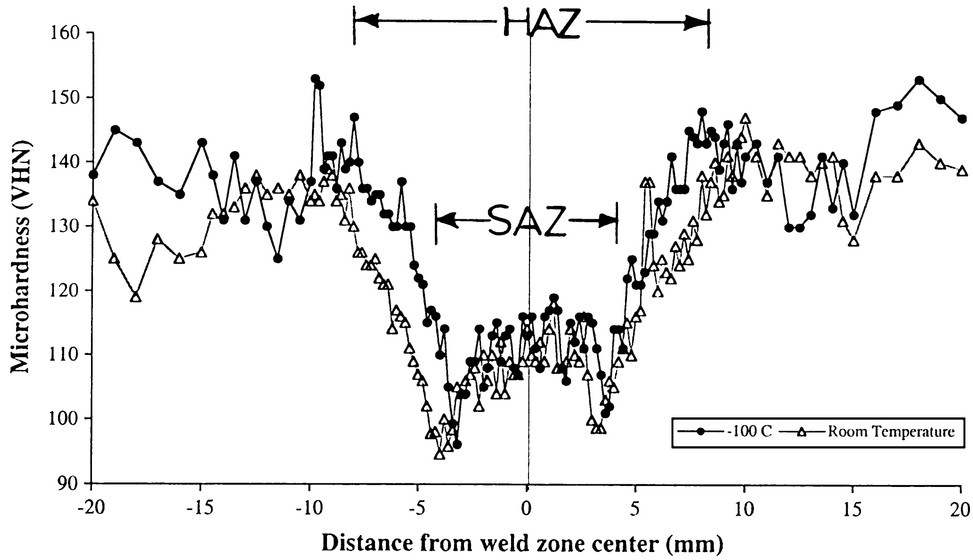

Fig. 3 Comparison of microindentation hardness profiles which traverse the weld center in Fig. 2(c) at room temperature and in Fig. 2(d) corresponding to FSW at −100 °C (R = 650 rpm, T = 1 mm/s); after Benavides et al. (Ref 20)

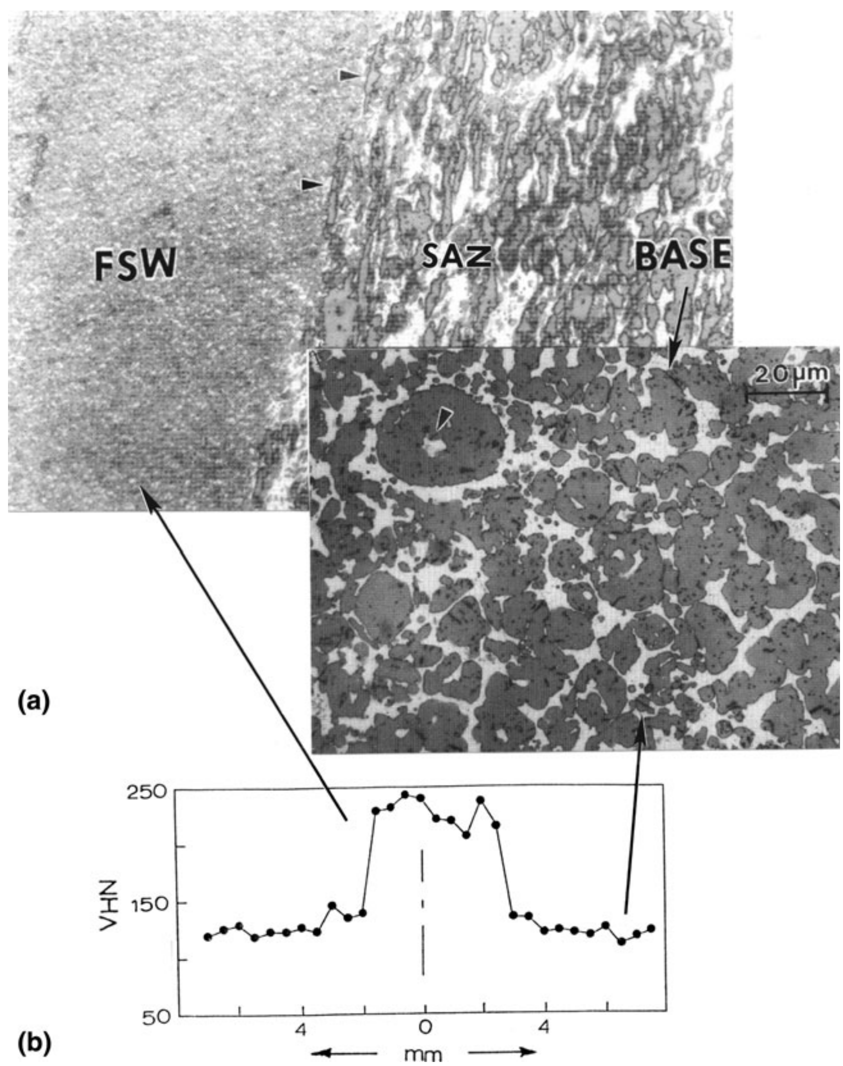

Fig. 4 FSW of Be 62-Al 38 composite. (a) The weld zone (FSW), stir-affected zone (SAZ), and base plate microstructure consisting of Be particles in an aluminum matrix. (b) The microindentatioan hardness profile through the weld center (*top-to-bottom*) for an FSW tool speed of 1000 rpm (counter-clockwise) and tool traverse speed of 1 mm/s; after Ref 21

produce significant hardening in the weld zone, also as a consequence of microstructural changes. A particularly notable example is provided in the FSW of a 62Be-38Al composite (or 2-phase system), also known as AlBeMet® AM16 (Ref 21). As illustrated in Fig. 4, the FSW of this composite produces fine, DRX (solid-solution) grains in the weld zone (shown at FSW in Fig. 4a) giving rise to hardening by nearly a factor of 3 as illustrated in the VHN profile through the weld center corresponding to the hardness profiles in Fig. 3. This hardening occurs because the hard Be particles suspended in the Al matrix are stirred into a continuous alloy with the small DRX grain structure having contiguous and homogeneous (or uniformly distributed) Be-Al grains as illustrated in Fig. 5. This structure is a mechanically alloyed solid-solution where the melting

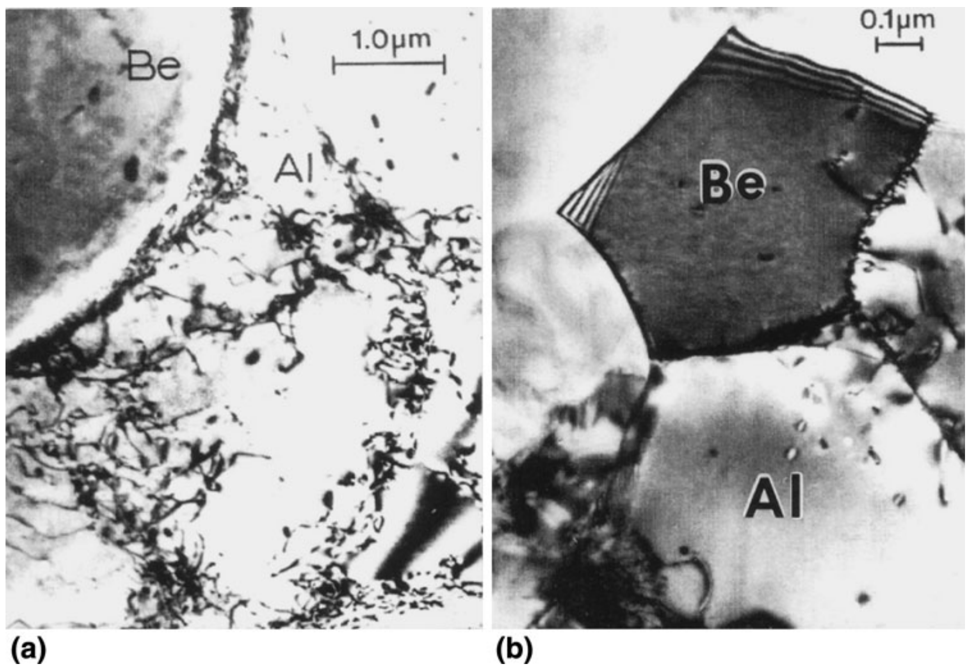

Fig. 5 TEM views of microstructures in the unwelded Be62-Al38 base plate (a) and the weld center (Fig. 4a) after FSW; after Ref 21

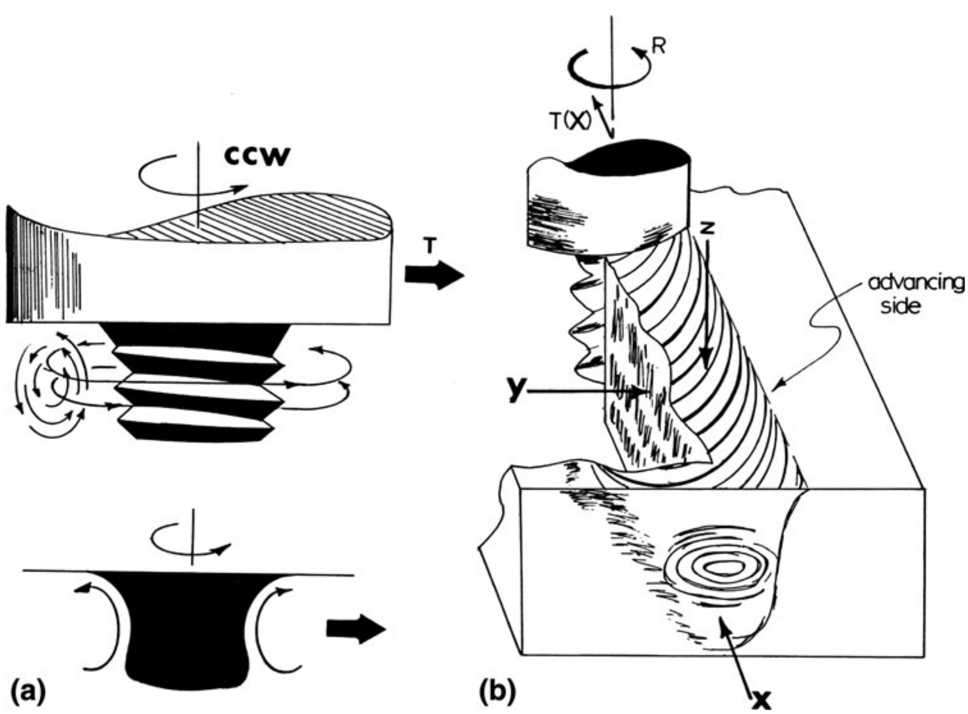

Fig. 6 Schematic views of solid-state flow and flow features associated with tool rotation (a) and traverse (b). The tool rotation illustrated is counter-clockwise (ccw)

point is around 1080 °C in contrast to the original two-phase system where the Al matrix melts at 660 °C while the Be particles melt at 1300 °C. In effect, this is tantamount to a dissimilar FSW system. The initial Be particles shown in the base or unwelded plate (or work piece) as illustrated in Fig. 4(a) are deformed into elongated and even refined Be particles in the SAZ transition from the weld zone boundary marked by arrows in Fig. 4(a). In contrast to the complex structure in the weld face for the FSW of Al 2024 to Ag in Fig. 1(d), the FSW of the Be-Al system exhibits the same uniformity as the FSW of Al 1100 in Fig. 2(a) and Al 2024 in Fig. 2(c) and (d). This points up the complexity of solid-state flow and mixing for the FSW of dissimilar materials in contrast to the FSW of a single base or single component material.

In many systems, the welding parameters (R and T in Fig. 1a) may produce turbulence within the weld zone giving rise to intercalated vortices or so-called "onion ring" structures in the weld face as a consequence of the "solid fluid" motion produced by tool rotation and traverse, especially their velocities. These features are illustrated schematically in Fig. 6 which illustrates prominent flow lines associated with pin tool motion (rotation, R and traverse velocity, T) in Fig. 6(a), and the onion ring formation illustrated schematically in Fig. 6(b), which also shows a section view of the weld illustrating other, systematic structural features associated with

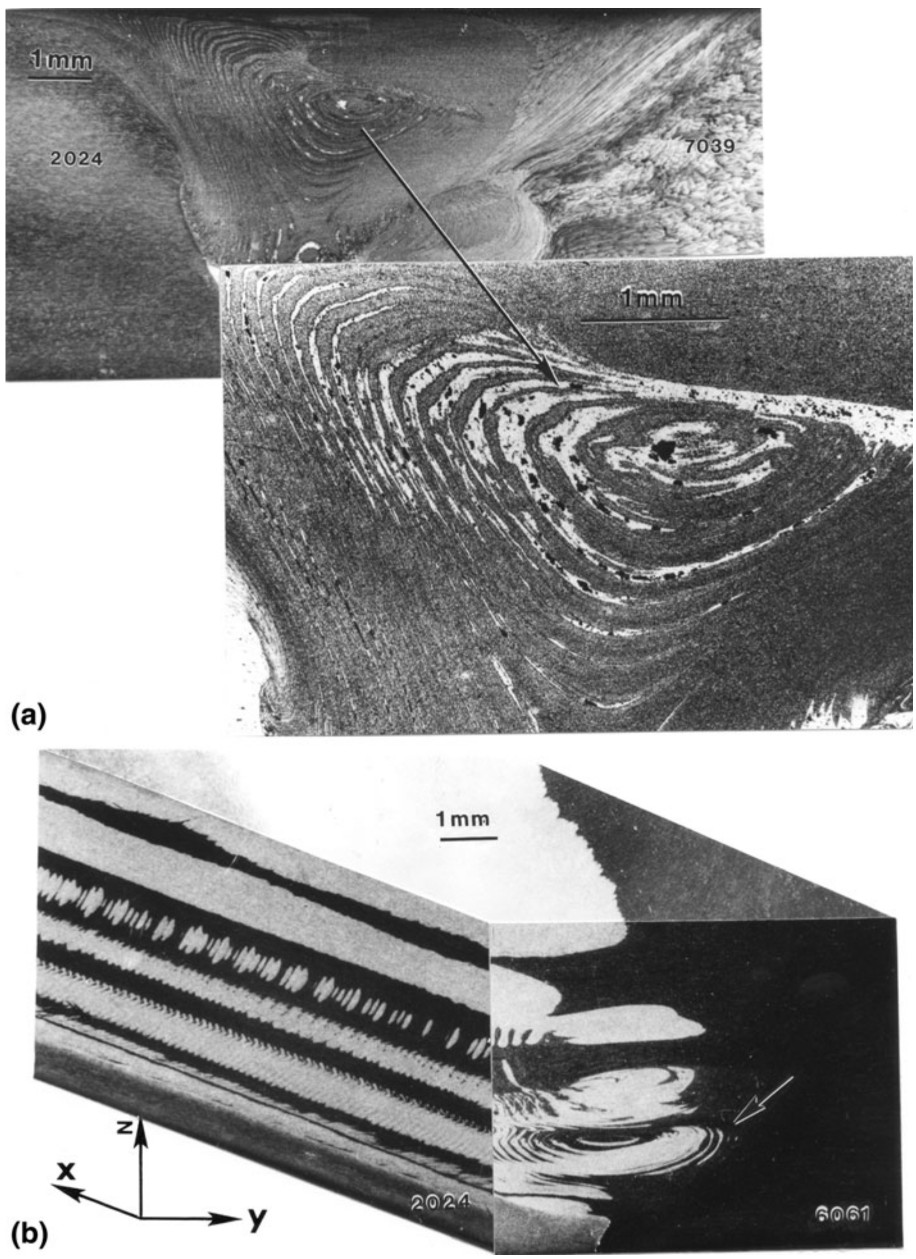

Fig. 7 Complex, intercalation flow patterns in the weld zone for dissimilar metals FSW. (a) Onion-ring-vortex-like structure in Al 2024/Al 7039 weld zone (800 rpm-1 mm/s, clockwise; Al 2024 advancing side); after Ref 22. (b) 3D weld section view of intercalation flow patterns for Al 2024 welded to Al 6061 at 400 rpm (R), 2 mm/s (T); after Ref 14

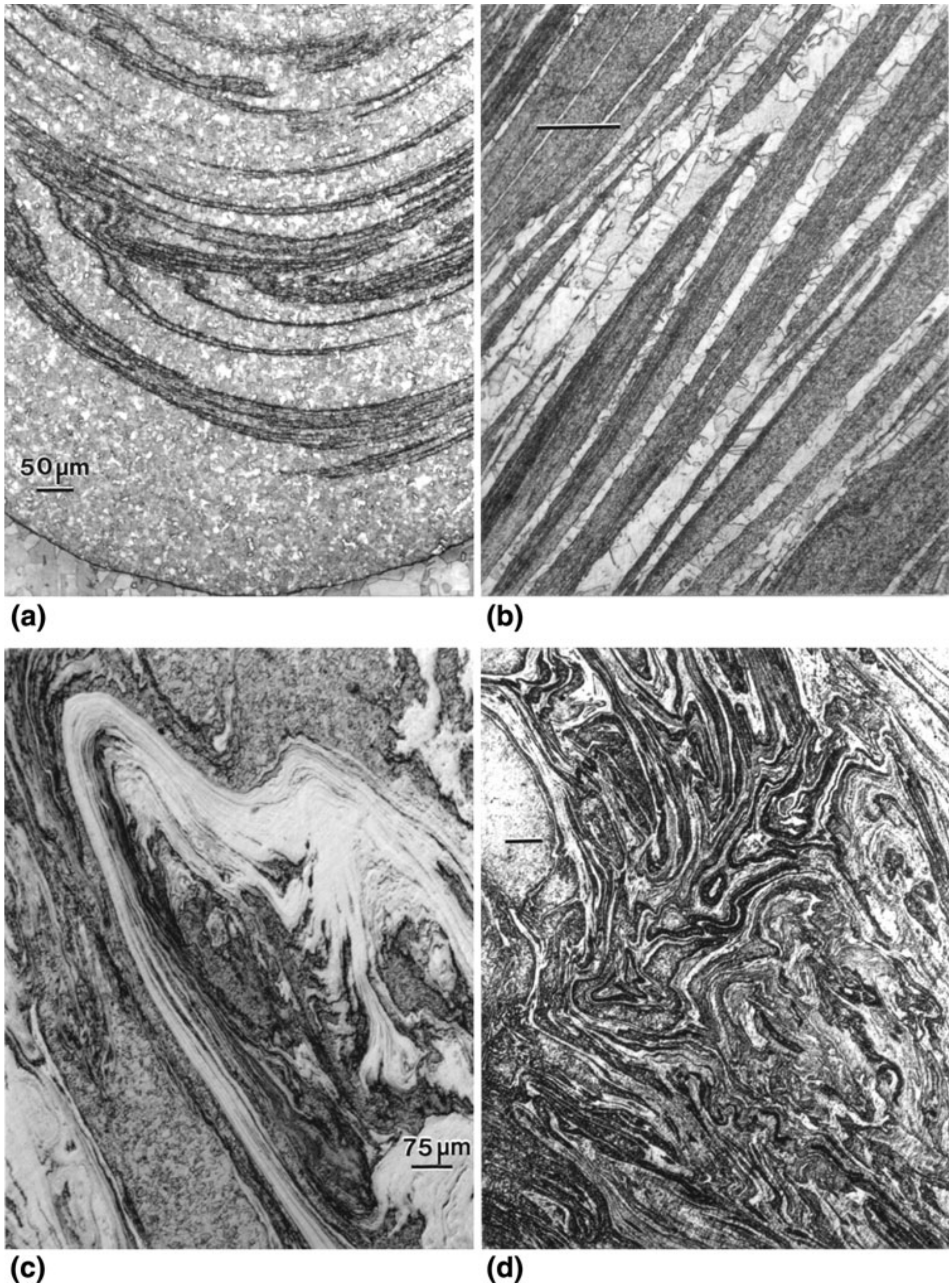

Fig. 8 Complex flow patterns for dissimilar metal FSW. (a) Cu/brass, (b) Cu/Ag. Both (a) and (b) are in the weld face plane (Fig. 1a-4). (c) Cu/Ag (weld/surface), (d) brass/Ag (weld surface). The weld surface is perpendicular to the *z*-axis in Fig. 1(a)-5

weld zone flow. In most of our studies we used a hardened, ¼-20 screw as the HP, and this design produces "fluid" turbulences different from other tool geometries. Figure 7 shows some examples of these complex flow features which are exaggerated for dissimilar materials FSW (Ref 22). Figure 7(a) shows onion ring structures within the weld zone for Al 2024 welded to Al 7039 while Fig. 7(b) shows more complex features for a section view of the FSW of Al 2024 to Al 6061. Note that in Fig. 7(b) the surface of the weld exhibits some stir features as a consequence of the chuck or shoulder rotation illustrated in Fig. 6(b). The surface (plane) structure is often much more complex than the weld face structure, especially for dissimilar materials FSW, and this is illustrated in Fig. 8 which shows a variety of dissimilar system welds: Cu/brass (70 Zn/30 Cu) in Fig. 8(a) and Cu/Ag in Fig. 8(b), both representing the weld face plane (Fig. 1(a)-4); brass/Ag in Fig. 8(c) and Cu/Ag in Fig. 8(d), both also representing the weld surface plane. Figure 8(d) is especially complex, exhibiting DRX flow in both the Cu and the Ag, with complex intercalated vortex and related flow features. It is interesting and notable that the differential etching, either of differently deformed, intercalated zones or in intercalated zones of different chemistry or elemental composition, creates residual visualizations of fluid-like, solid-state flow features similar to

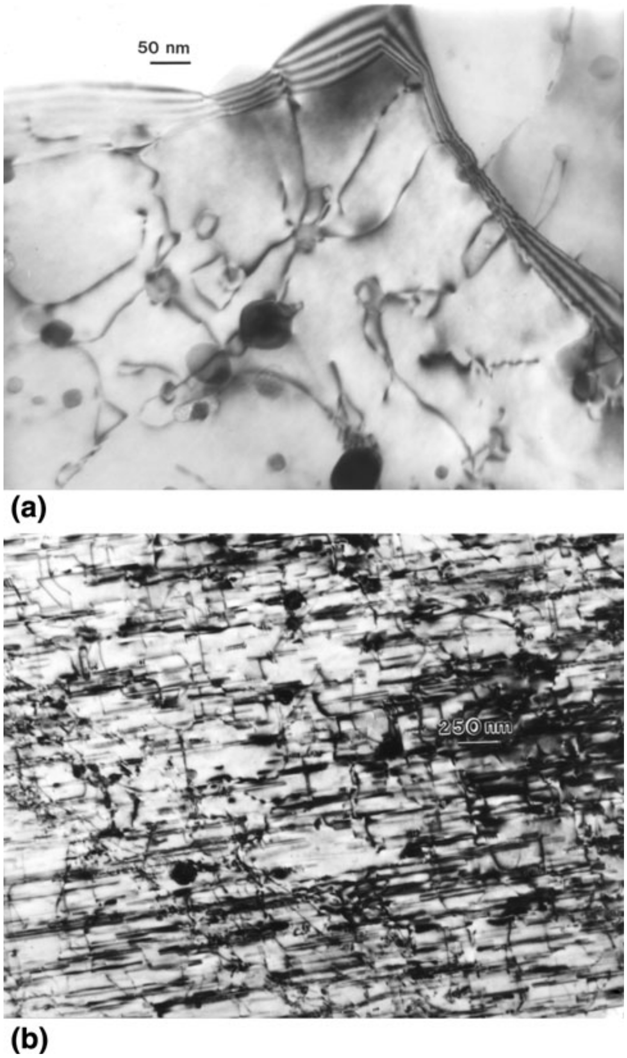

Fig. 9 Temperature-affected precipitation differences in the weld zone for FSW of Al 6061. (a) TEM image of precipitates near the top of the weld along with some residual dislocations. (b) Widmanstäten structure composed of Güinier-Preston zone precipitates and needle precipitates near the bottom of the weld

related, complex flow in gas and liquid turbulent mixing (Ref 23). The creation of vortex structures in solid-state flow regimes is particularly extraordinary.

2. Experimental Issues, Microstructures, and Hardness Results

The previous, introductory section has outlined the fundamental issues characteristic of FSW; utilizing examples for the FSW of the same base materials as well as dissimilar materials systems. These fundamentals have included microstructure and microstructure evolution (Fig. 1b) as well as microstructure comparisons. Figures 3 and 4(b) illustrate the use of residual microindentation and other potential hardness measurements across the weld face to monitor the weld behavior in relation to the unwelded base material. These weld face hardness profiles provide a "performance signature" for the FSW process as well as performance comparisons illustrated in Fig. 3. Figure 3 also illustrates, along with Fig. 4, the HAZ and the SAZ which, in addition to the DRX of the weld zone includes the deformation of the base material as a transition between the weld zone boundary and the base material. Correspondingly, a comparison of Fig. 3 and Fig. 4(b) illustrates opposing behavior in the weld zone which is due to the material behavior as it relates to microstructure, microstructure variations, or microstructure evolution within or near the weld zone.

Table 1 Same materials FSW systems and weld parameters

FSW system	Weld parameters: *R* (rpm)	*T* (mm/s)	Reference
Al 1100/Al 1100 (A)	400 (ccw)	2	(Ref 16, 25)
Al 1100 (a)/Al 1100 (a) (A)	400 (ccw)	2	(Ref 16, 25)
Al 2024/Al 2024 (A)	800 (ccw)	1	(Ref 16, 25)
Al 6061/Al 6061 (A)	400 (ccw)	2	(Ref 16, 25)
Al 2195/Al/2195 (A)	800 (ccw)	1	(Ref 16, 25)
Al 7075/Al/7075 (A)	1250 (ccw) (b)	1	(Ref 15)
Al 2017/Al 2017 (A)	1250 (ccw)	1	(Ref 15)
Al 5052/Al 5052 (A)	1250 (ccw)	1	(Ref 15)
Cu/Cu (A)	1000 (ccw)	1	(Ref 31)
Brass (70-30)/brass (A)	1000 (ccw)	1	(Ref 31)
Ag/Ag (A)	1000 (ccw)	1	(Ref 31)
Al 6061 + 20% Al_2O_3/ Al 6061 + 20% Al_2O_3 (A)	650 (ccw)	1-9	(Ref 9, 16)
Al 339 + 10% SiC/Al 339 + 10% SiC (A)	650 (cw)	1	(Ref 16)
Al 359 + 20% SiC/Al 359 + 20% SiC (A)	1000 (ccw)	1-9	(Ref 9)
62 Be-38 Al/62 Be-38 Al (A)			
AZ 31B/AZ 31B (A)	800 (ccw)	1	(Ref 29)
AM-60/AM-60	2000 (cw)	2	(Ref 28)
AZ 91D/AZ91D (A)	800 (ccw)	1	(Ref 29)

(a) Columnar grain: see Fig. 2(a)
(b) Smaller pin tool (4.6 mm diameter, 2.58 mm long)

Tang et al. (Ref 24) have shown that the maximum temperature rise for FSW of Al 6061 was about 0.8 T_M (T_M = melting point equal to roughly 580 °C for Al 6061). Murr et al. (Ref 25) have also shown that the mid-weld temperature during FSW of Al 2024 to Al 6061 increases from roughly 0.7 T_M at a tool rotation speed of 300 rpm to 0.8 T_M at a tool rotation speed of 1,000 rpm for a pin tool (or head pin, HP) traverse of 1 mm/s. In addition, temperatures vary from the top to bottom of the weld as well as from the weld centerline (Fig. 1(a)-4); with higher temperatures at the top of the weld and along the weld centerline. For age hardenable alloys such as Al 6061 and 2024, this produces a wide range of evolving microstructures, particularly precipitation and precipitate evolution which is associated with corresponding hardness within the weld zone. For aluminum alloys such as Al 6061, the weld zone following FSW contains every possible precipitation feature from Güinier-Preston zones to Widmanstätten structures to mixtures of regular precipitates, ranging in size or dimension from 10 to 1000 nm (Ref 26). Figure 9 illustrates these features generally for regions near the top (Fig. 9a) and bottom (Fig. 9b) of the weld zone in Al 6061 FSW. Temperature rise is also associated with traverse speed, increasing for increasing traverse speed. Increasing the welding pressure (pressure on the pin tool) increases the temperature, especially under the tool holder (or chuck), referred to as the shoulder of the pin tool. This effect spreads the upper (top) portion of the weld zone and creates complex flow features in contrast to the weld zone as shown in Fig. 8. Correspondingly, the tool rotation speed (*R*) and traverse speed (*T*) need to be optimized in many FSW processes in order to produce a good weld, free of defects, especially weld tunnels which often traverse the full length of the weld. In the examples in this paper, *R* and *T* are not necessarily optimized although in some studies they have been systematically adjusted to produce the best weld features (Ref 27, 28).

Table 2 Dissimilar materials FSW systems and weld parameters

FSW system	Weld parameters: *R* (rpm)	*T* (mm/s)	Reference
Al 2024/Al 1100 (A) (a)	800 (ccw)	1	(Ref 25)
Al 2024/Al 6061 (A)	800 (ccw)	1	(Ref 25)
Al 2024/Al 2195 (A)	800 (ccw)	1	(Ref 25)
Cu/brass (A)	650 (ccw)	1	(Ref 16)
Al 2024/Cu (A)	650 (ccw)	1	(Ref 16)
Al 6061Cu	650 (cw)	1	(Ref 16)
Ag/brass	1000 (ccw)	1	(Ref 31)
Cu/brass	1000 (ccw)	1	(Ref 31)
Cu/Ag	1000 (ccw)	1	(Ref 31)
Ag/Al 2024 (A)	650 (ccw)	1	(Ref 16)
Al 7075/Al 5052 (A)	1250 (ccw)	1	(Ref 15)
Al 2017/Al 5052 (A)	1250 (ccw)	1	(Ref 15)
Al 2024/Al 7039 (A)	800 (ccw)	1	(Ref 22)
Al 7075/Al 2017 (A)	1250 (ccw)	1	(Ref 15)
Al 5052/Al 7075 (A)	1250 (ccw)	1	(Ref 15)
Al 5052/Al 2017 (A)	1250 (ccw)	1	(Ref 15)
A 1 2017/Al 7075 (A)	1250 (ccw)	1	(Ref 15)
Al 7075/Al 1100 (A)	1250 (ccw)	1	(Ref 15)
Al 1100/Al 7075 (A)	1250 (ccw)	1	(Ref 15)
Al 6061 + 20% Al_2O_3/ Al 339 + 10% SiC (A)	800 (ccw)	1	(Ref 16)
Al 6061 + 20% Al_2O_3 Al 359 + 20% SiC (A)	1000 (ccw)	1	...
AZ 91D (A)/Al 6061 (A)	800 (ccw)	1.5	(Ref 30)
Al 6061 (A)/AZ31B	800 (ccw)	1.5	(Ref 30)
AZ31B (A)/Al 6061	800 (cw)	1.5	(Ref 30)
Al 7x1/Al 7x5x (A) (scandium alloy)	1000 (ccw)	1	(Ref 27)

(a) The advancing side is denoted (A)

Tables 1 and 2 illustrate the FSW systems investigated at the University of Texas at El Paso (UTEP) since 1996. These systems have involved nominally 0.62 cm thick butted base plates (Fig. 1a) welded using a ¼-20 hardened screw slightly shorter than the base plates (~0.6 cm), and 1 to 2° tilt (or lead angle). Values of *R* and *T* in Tables 1 and 2 are not, as noted above, necessarily optimized. While Table 1 lists FSW of the same base materials, it is useful to have a reference for FSW for specific components composing dissimilar welds as noted in Table 2. Tables 1 and 2 also indicate the FSW parameters (pin tool rotation, *R*, and traverse, *T*). Table 3 shows the nominal composition for each of the materials investigated (Table 1).

Figure 10 illustrates the comparative microindentation hardness profiles in the weld face (Fig. 1(a)-4) for the first five materials in Table 1, as well as dissimilar materials combinations (Ref 25). The actual weld zone extent through the weld centerline and at the weld mid-point (top-to-bottom) is indicated by arrows. For the Al 2024, 6061, and 2195, there is a notable HAZ which results from aging and precipitation variations within this zone as noted very generally for Al 6061 in Fig. 9. The very wide and relatively flat weld zone and HAZ observed for Al 2195 is the result of coherent Al_2CuLi precipitate dissolution as illustrated generally in Fig. 11. The softening observed for FSW of Al 2195 in Fig. 10 results more from the loss of precipitates than DRX (Fig. 11). The difference

Table 3 Nominal chemical composition (wt.%) for FSW materials

Material	Component (wt.%): Ag	Be	Cr	Cu	Fe	Li	Mg	Mn	Ni	Sc	Si	Ti	Zn	Zr	Al
1100	...	...	...	0.15	0.5	...	...	...	...	...	...	0.04	...		Bal.
2017	...	...	...	4.0	...	...	0.6	...	...	...	...	...	...		Bal.
2024	...	...	...	4.5	...	...	0.5	0.3	...	...	...	...	...		Bal.
2052	...	...	...	...	...	...	2.5	...	...	...	...	...	...		Bal.
2195	0.4	...	...	4.0	...	1.0	0.5	0.3	...	...	...	...	...		Bal.
6061	...	...	0.2	0.25	...	...	1.0	...	...	...	0.6	...	...		Bal.
7039	...	...	0.2	...	...	...	2.8	0.3	...	...	...	...	4.0		Bal.
7075	...	...	...	1.6	...	...	2.5	...	...	...	...	...	5.6		Bal.
7x1x	...	...	...	1.9	...	...	2.2	...	...	0.1	...	0.06	5.2	0.12	Bal.
7x5x	...	...	...	0.3	...	...	2.0	...	...	0.1	...	0.03	8.1	0.14	Bal.
A339	...	...	...	1.0	...	...	1.0	...	1.0	...	11.0	...	...	...	Bal.
A359	...	...	...	0.2	...	...	0.5	...	...	...	9.0	0.2	...	...	Bal.
AlBeMet®	...	61.5	...	...	...	...	...	...	...	...	...	...	...	...	Bal.
Copper	...	...	...	99.9	...	...	...	...	...	...	...	...	...	...	...
Brass	...	...	...	70.0	...	...	...	...	...	...	...	...	30.0	...	...
Silver	99.9	...	...	...	...	...	...	...	...	...	...	...	...	...	...
AZ31B	...	...	...	0.04	...	...	Bal.	0.6	...	...	0.1	...	1.0	...	3.0
AZ91D	...	...	...	0.03	...	...	Bal.	0.35	...	...	...	...	0.65	...	6.0
AM60B	...	...	...	0.01	...	...	Bal.	0.42	...	...	0.1	...	0.22	...	6.0

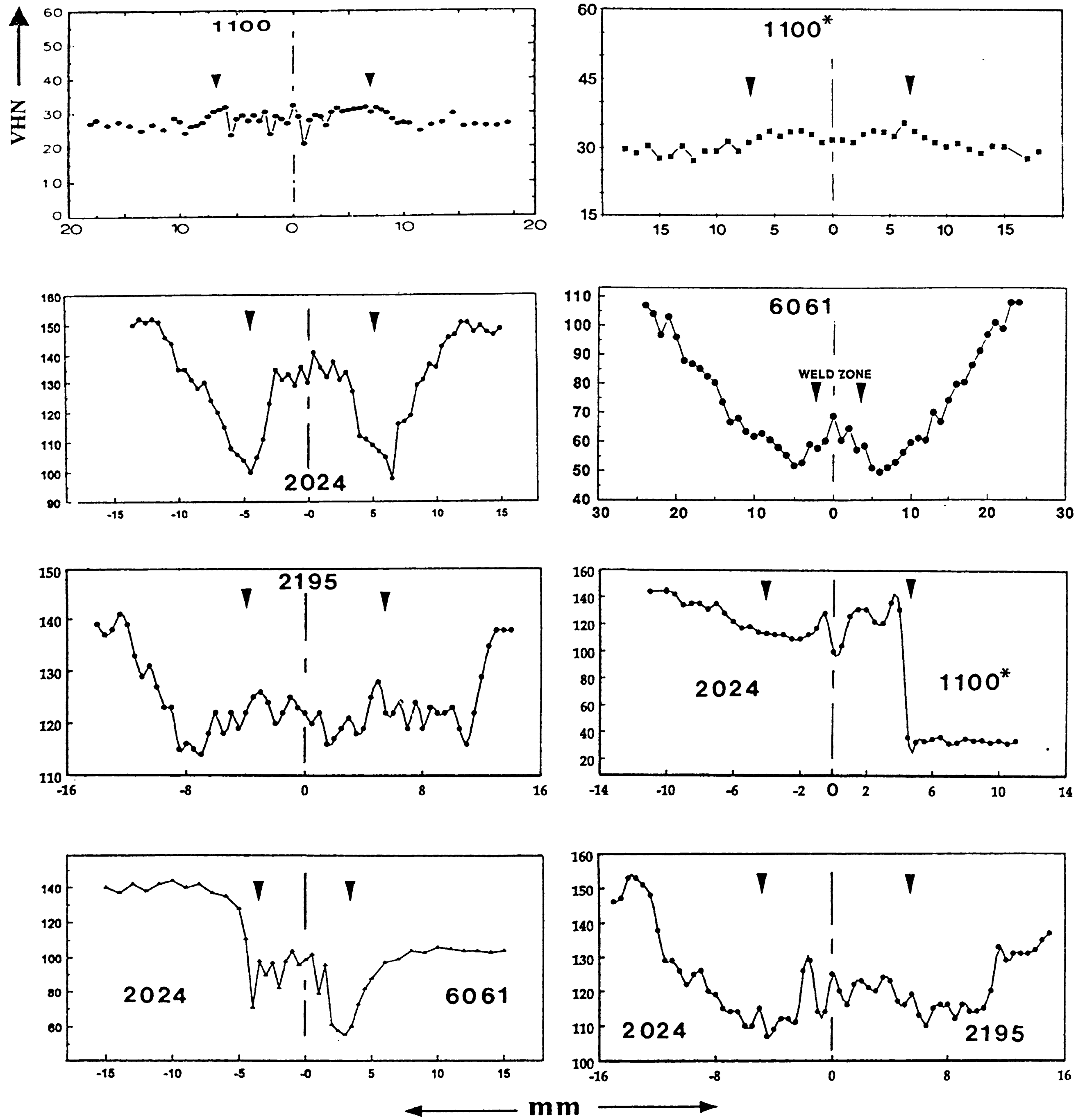

Fig. 10 Weld zone/weld face residual (Vickers) microindentation hardness profiles for a number of same and dissimilar aluminum alloy welds. The arrows denote the weld zone boundaries at mid-weld; from Ref 25. The Al 1100 weld is for the cast, columnar grained material shown in Fig. 2(a)

between the FSW of Al 2195 and Al 2024 and dissimilar Al 2024/Al 2195, is the general trend toward Al 2195 within the weld zone while the edges of the HAZ for the retreating Al 2024 side and the advancing Al 2195 reflect the features of FSW for each of these component work pieces (base plates). It can be noted that there is a very similar intercalation structure for the Al 2195 and the dissimilar Al 2024/Al 2195 system as illustrated in Fig. 12.

The complex, intercalated flow which is a characteristic especially for many dissimilar materials FSW systems (Table 2) causes fluctuations in microindentation hardness profiles, especially in the weld zone, but often in the region at the edges of the weld zone, depending on the advancing versus retreating side materials. This feature is implicit in the microstructures shown in Fig. 8 and explicit on comparing the corresponding microindentation hardness profiles reproduced in Fig. 13 and 14, especially on comparing the FSW for the same material (such as Cu and brass in Fig. 13), with the dissimilar Cu/brass FSW system. Similar features are shown for the Ag/brass and Cu/Ag systems in Fig. 14, and Fig. 15

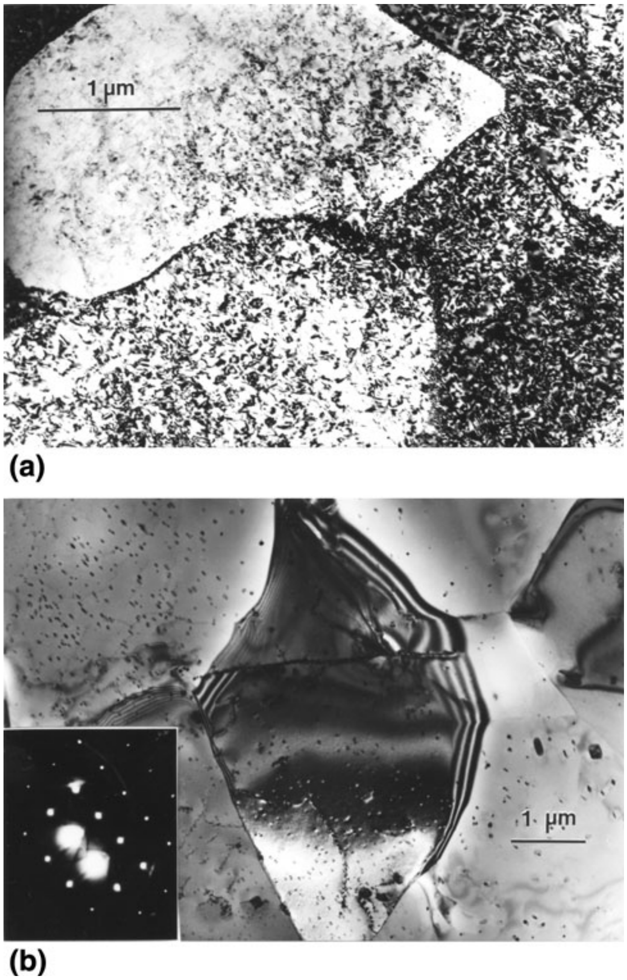

Fig. 11 Precipitation differences from the base alloy (a) and the weld zone center (b) for the FSW of Al 2195 observed by TEM. The selected area electron diffraction pattern insert in (b) is [001], representing the dark grain in the image center

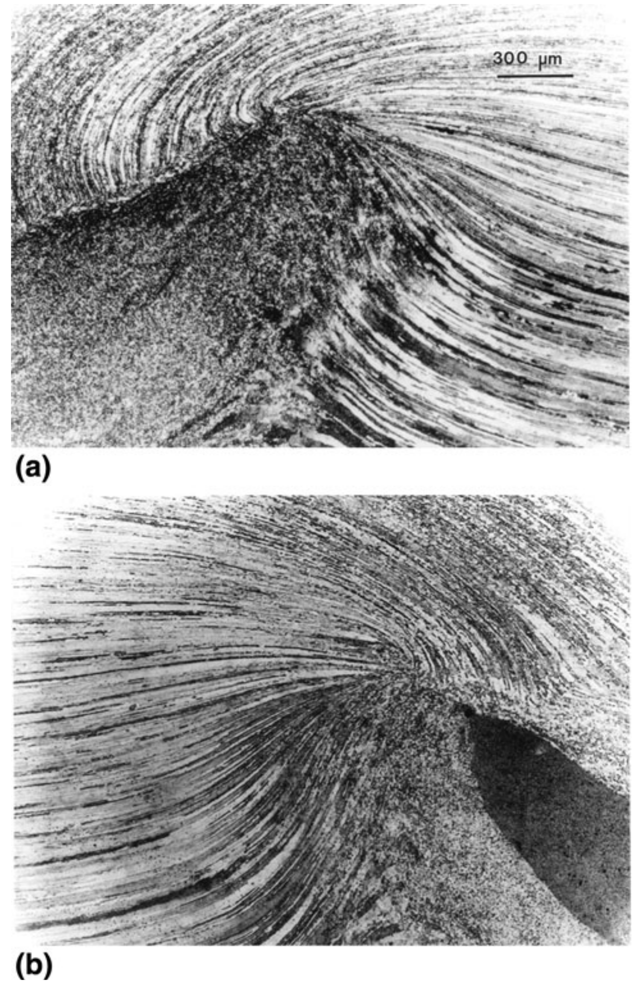

Fig. 12 Weld zone intercalation structures separating the weld zone and the SAZ for the same Al 2195 FSW in (a) and the dissimilar Al 2024/Al 2195 dissimilar FSW system in (b)

illustrates corresponding, complex, intercalated weld face microstructures for the Cu/Ag dissimilar FSW systems. The microstructures characteristic of the initial, unwelded base plates and the complex flow patterns for the weld zone for the Ag/Al 2024 FSW system in Fig. 14 were illustrated initially in Fig. 1(c) and (d), respectively. These complex, intercalation features are dependent upon the direction of stirring (cw versus ccw) or the alternation of the work pieces (A/B versus B/A) for a constant rotation direction. These features are illustrated for Al 7075, Al 2017, and Al 5052 (Table 3) in Fig. 16 as well as dissimilar Al 7075/Al 1100 FSW shown in Fig. 17 where the notable spikes in weld face microindentation hardness occur on one side of the weld centerline or the other. The Al 7x1x/Al 7x5x in Fig. 17 is a scandium precipitation system similar in some respects to the Al 2024/Al 2195 system shown in Fig. 10.

There are interesting hardness profile features for dissimilar systems composed of precipitation hardenable components such as Al 2024/Al 1100 FSW in Fig. 10 and Ag/Al 2024 FSW in Fig. 14, where the Al 1100 and Ag are not precipitation hardenable in contrast to the Al 2024. This feature is exaggerated for the Al 6061 + 20% Al_2O_3/A339 + 10% SiC system shown in Fig. 18(c) where the aluminum alloy A339 is not precipitation hardenable like the Al 6061 and Al 6061 + 20% Al_2O_3 shown in Fig. 18(a) and (b), respectively, as a consequence of thermal (aging) treatment in contrast to hardening by non-coherent SiC particles. In these MMC systems; (Ref 9, 10), the hard particles (Al_2O_3 and SiC) are simply stirred homogeneously into the weld zone (Fig. 19) in contrast to the precipitation variations which occur for the Al 6061 matrix in the weld or HAZ (Fig. 9). Figure 19(b) shows only a small reduction in the weld zone grain size in contrast to the Al 6061 + 20% Al_2O_3 base material (Fig. 19a while Fig. 19c illustrates the homogeneous mixing of Al_2O_3 and SiC particles within the weld zone for the dissimilar MMC, FSW system (Fig. 18c)).

Esparza et al. (Ref 28, 29) and Somasekharan and Murr (Ref 33-35) have described the FSW of magnesium alloys (AM600, AZ31B, and AZ91D), dissimilar magnesium alloys (AZ91D/AM60D), and magnesium alloys to aluminum alloy 6061 (AZ91D/Al 6061, AZ31B/Al 6061) (Table 3). These FSW system hardness profiles are shown for comparison in Fig. 20 and 21.

Magnesium alloy AM 60 is a thixomolded alloy which can have varying solid fractions of the primary phase α-Mg. Figure 20(b) compares the FSW for 3% and 18% solid fraction

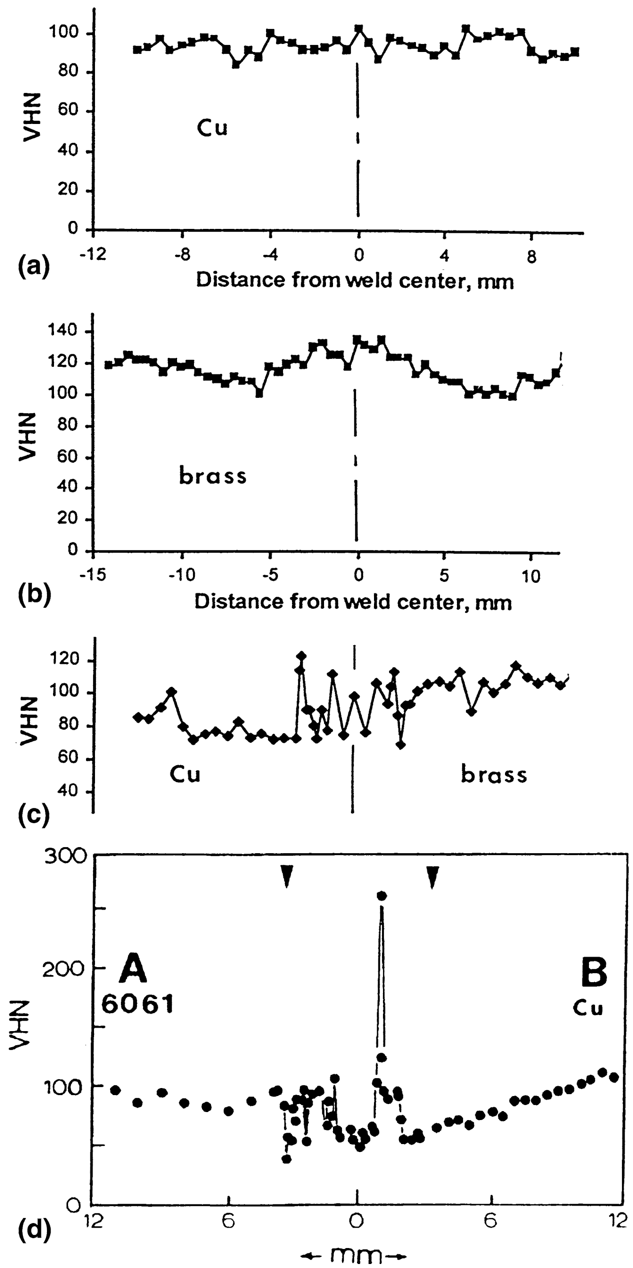

Fig. 13 Weld zone/weld face residual (Vickers) microindentation hardness profiles for a number of metal and alloy FSW systems. The Cu and brass data (a) and (b) is from Ref 31 while the dissimilar system FSW profiles in (c) and (d) are from Ref 32. *Arrows* in (d) indicate the weld zone at the weld mid-point

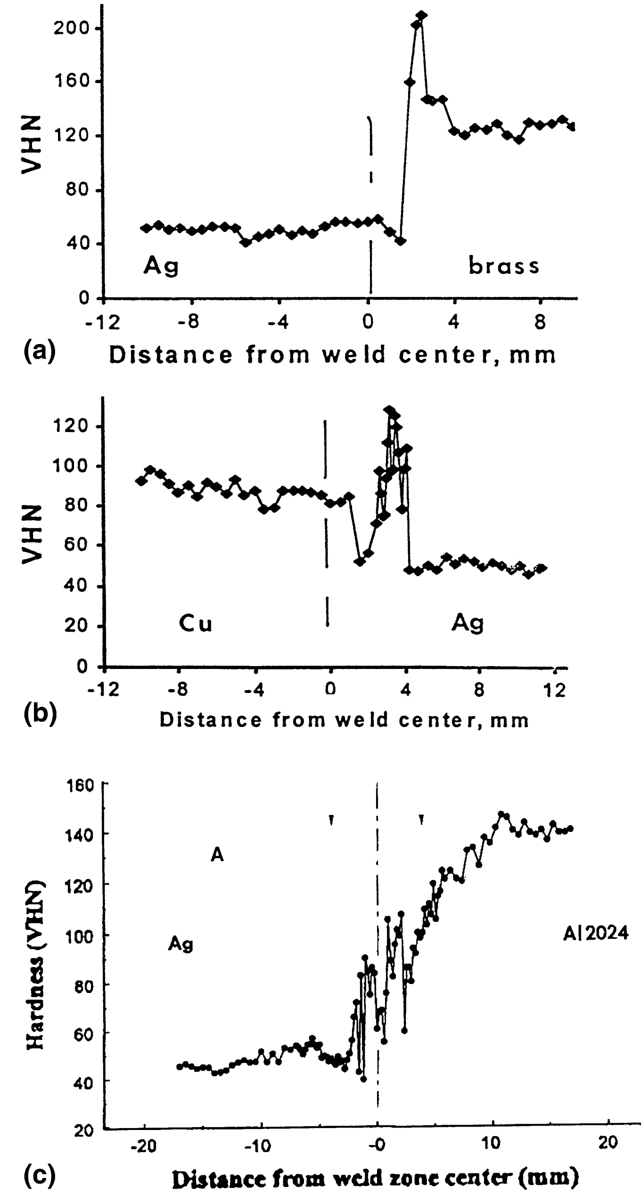

Fig. 14 Weld zone/weld face residual (Vickers) microindentation hardness profiles for dissimilar system FSW. (a) Ag/brass, (b) Cu/Ag, (c) Ag/Al 2024. *Arrows* in (c) indicate the mid-weld dimension. (d) An optical metallographic view for brass/Ag in the weld face plane

AM60. AZ31B and AZ91D are wrought magnesium alloy products (Table 3) which, as illustrated in Fig. 20(a), do not exhibit any precipitation hardening. Consequently, the FSW of dissimilar AZ91D/AM60D as shown in Fig. 20(c) for varying α-Mg solid fractions does not exhibit any significant weld zone variations despite the fact that DRX occurs in the weld zone, and complex, intercalation structures are created. However, even more complex, intercalation weld zone structures occur for the FSW of AZ91D/Al6061 and AZ31B/Al 6061 dissimilar systems and these exhibit very erratic hardness profiles as illustrated in Fig. 21. Moreover, there is a shift of erratic hardness features from one side of the weld center line when the base materials are reversed for a uniform pin tool rotation (ccw) as shown in comparing Fig. 21(b) and (c) which, as also illustrated in Fig. 21(a), show hardness variations near the top of the weld (at a), at the weld mid-point (at b) and at the bottom of the weld zone (at c).

3. Discussion and Conclusions

The salient features of FSW of dissimilar metals and alloys was illustrated and summarized at the outset in Fig. 1. Figures 3 and 4(b) also summarize the contrasting effects of

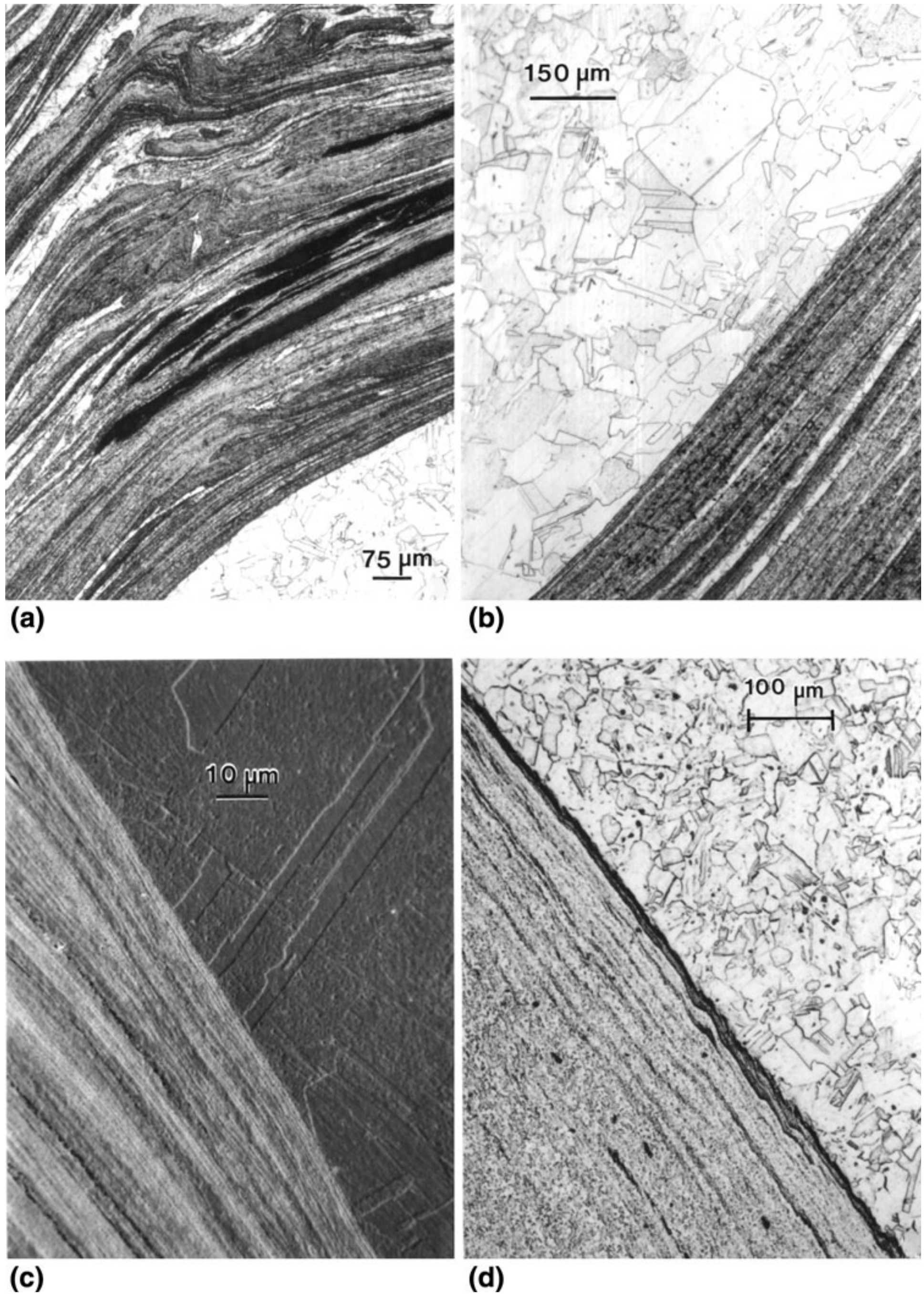

Fig. 15 Complex flow and intercalation patterns for dissimilar systems FSW. All views are in the weld face plane. (a, b) Two similar Cu/Ag locations in the weld face plane. (c) An SEM view of Cu/Ag in the weld face plane. (d) Brass/Ag in weld face plane

softening or hardening in the weld zone implicit in the residual microindentation (or other indentation) hardness profiles in the context of FSW for the same metal or alloy system. As shown in Fig. 10, the principal difference in the FSW of the same system of metals and alloys versus dissimilar system FSW is the variation in asymmetry or the degree of symmetry with reference to the weld centerline at zero of the residual hardness profiles for dissimilar system FSW. This is apparent on comparing the Al2024/Al100, Al2024/Al6061, and Al2024/Al2195 dissimilar system hardness profiles in Fig. 10. This feature is also illustrated in Fig. 14, 16, 17(a) and (b), and 21(b) and (c). As shown in Fig. 16 and 21(b) and (c), this hardness profile asymmetry is observed irrespective of the rotation direction (cw or ccw) or the advancing side (left or right): A or B in Fig. 1(a)-1. These contrasting features are also illustrated for aluminum MMC FSW as shown in Fig. 18(c).

Regardless of the FSW system, the fundamental process involves DRX-facilitated, solid-state flow. The material flow can produce complex, lamellar, or vortex-like patterns even in the FSW of the same materials, as a consequence of intercalated

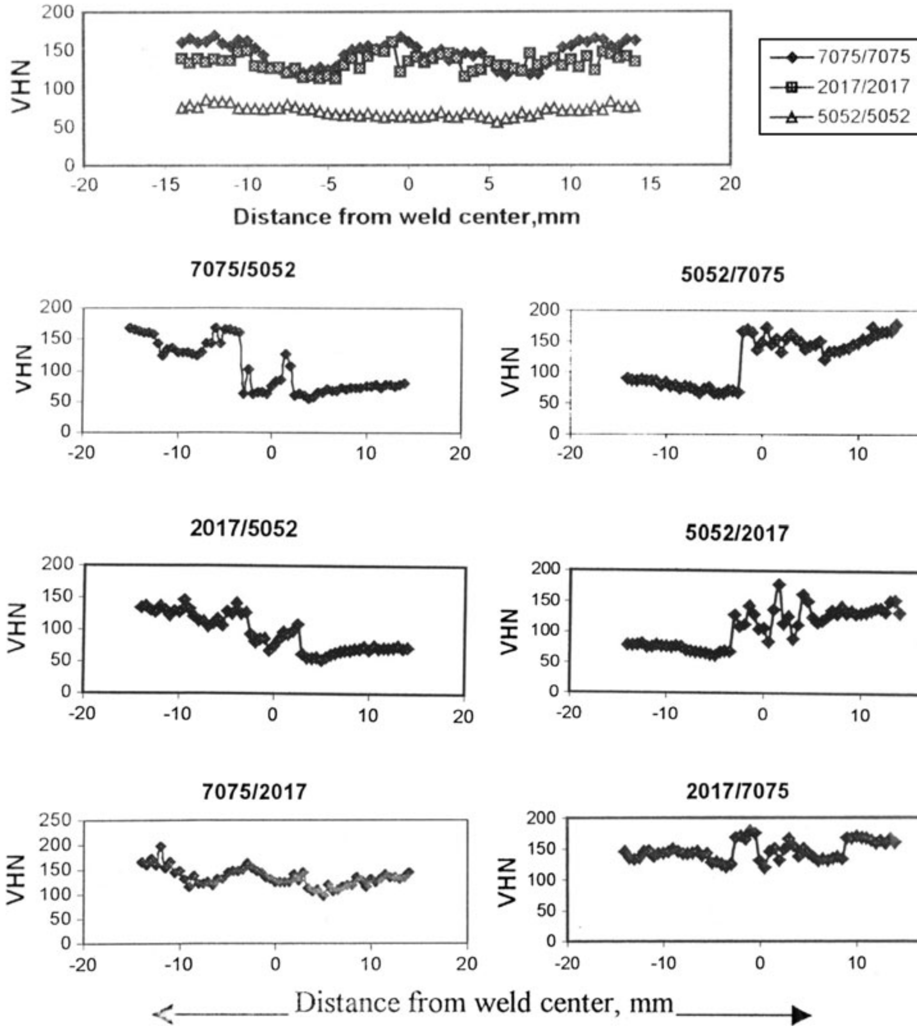

Fig. 16 Comparison of weld face residual (Vickers) microindentation hardness profiles for a number of aluminum alloy FSW systems; from Ref 15

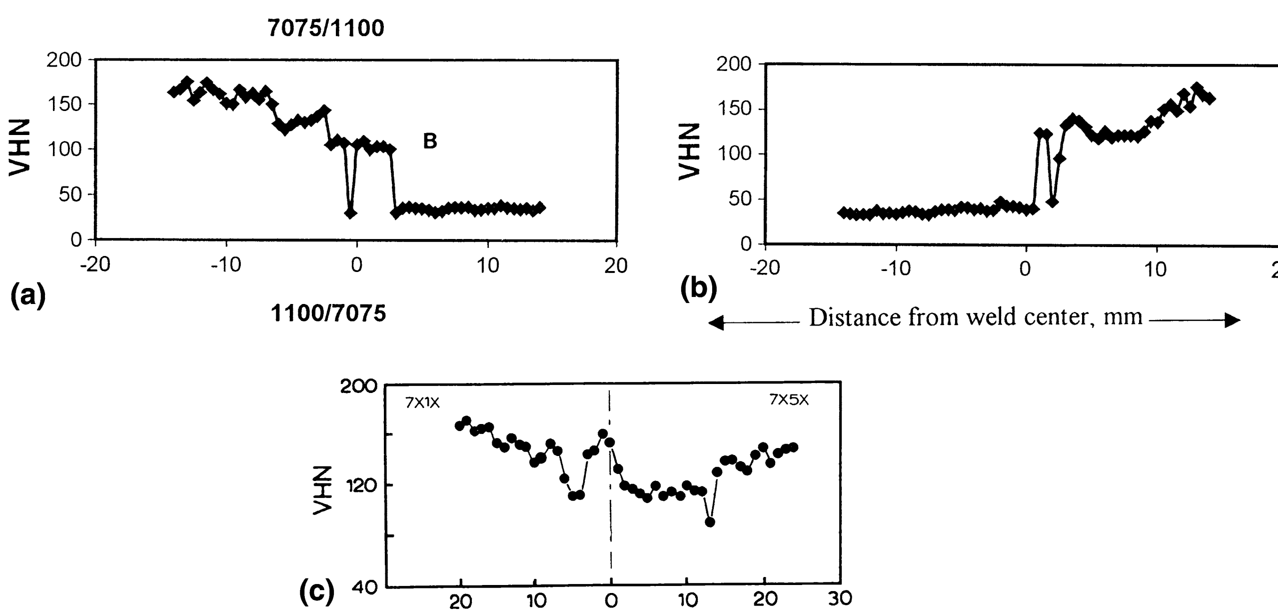

Fig. 17 Comparison of weld face residual (Vickers) microindentation hardness profiles for Al 7075/Al 1100 dissimilar systems in (a) and (b), and Al 7x1x/Al/7x5x (scandium precipitation) system following FSW. (a) and (b) are from Ref 15, (c) is from Ref 16

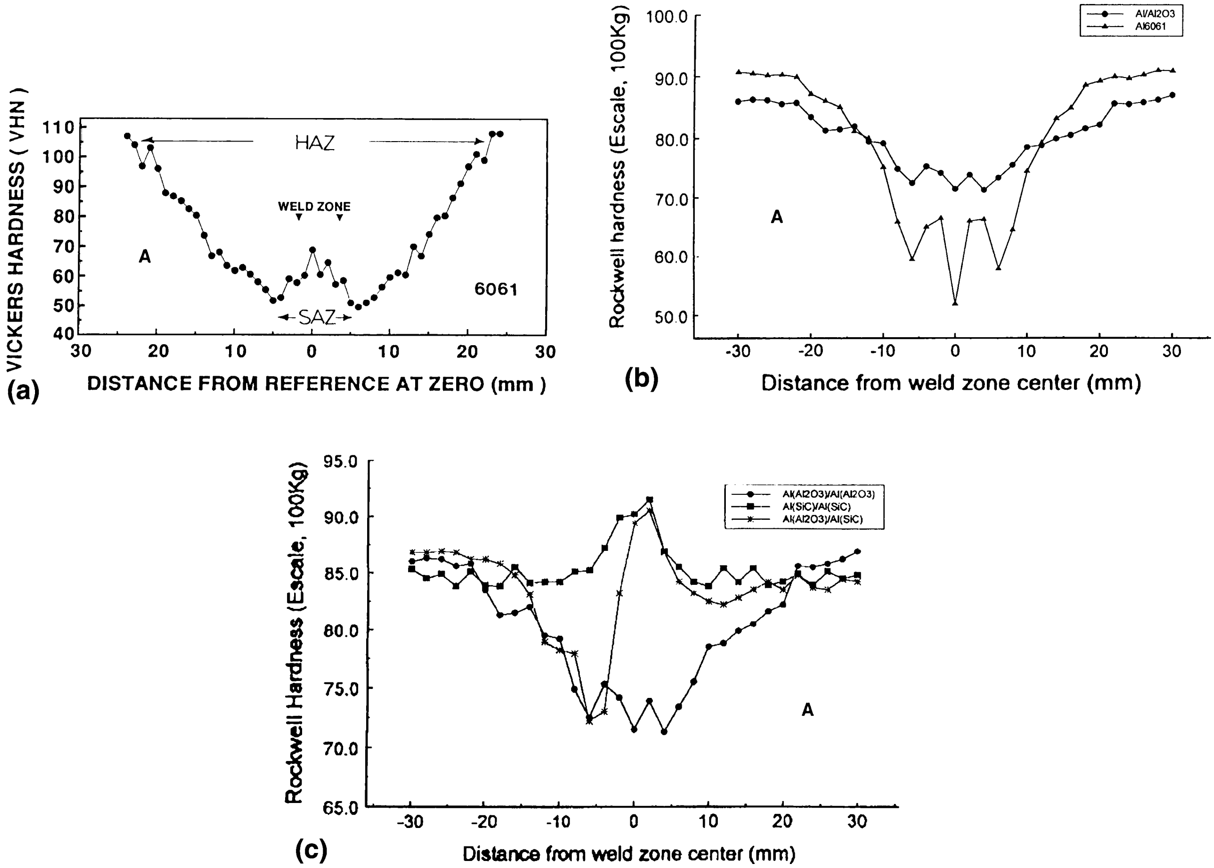

Fig. 18 Comparison of residual hardness profiles for Al 6061 FSW (a), Al 6061 + 20% Al_2O_3 FSW (b), and Al 6061 + 20% Al_2O_3 with A339 + 10% SiC, and the dissimilar FSW system—Al 6061 + 20% Al_2O_3/A339 + 10% SiC (c); from Ref 16. Note the hardness in (b) and (c) was Rockwell E-scale

regions of different hardness or degree of DRX, and especially in dissimilar system DRX where intercalation of the different base materials occurs. These complex, intercalation patterns are observed in Fig. 1(d), 7, 8, 12, and 15. Figure 8 is particularly interesting because it provides a contrast from the weld face flow (Fig. 8a and b) and mixing, to the weld surface (Fig. 8c and d), where the chuck (or tool shoulder) contributes to the DRX and flow process. These complex intercalation patterns contribute to the hardness profiles because they alter the microstructural spacing and structure which account for the hardness variations. Consequently, as shown in Fig. 13(c) and 14(a) and (b) in particular, as compared with corresponding weld face flow patterns, hardness fluctuations are related to the flow pattern structures. This feature is also implicit on examining Fig. 15 as well.

In this short review of FSW systems and associated hardness responses, melting points for individual metals or alloys ranged from roughly 550 to 1300 °C for the Be particle phase in the 62 Be-38 Al, two-phase composite, and this temperature range has been extended with high-temperature tooling to roughly 1600 °C for Ti and Ti-alloys (Ref 6, 7). As illustrated generally in this review, a host of unweldable systems (by fusion welding) can be effectively joined by FSW, without melt. In fact, it appears that essentially any dissimilar metal or alloy system can be joined by FSW, including contrasting temperature systems: Fig. 4 for the two-phase Be-Al (1300-660 °C) is a case in point. Similarly, aluminum MMCs—Al + Al_2O_3 and Al + SiC are another example of the joining advantage offered by FSW, whether the joining involves the same material or dissimilar material. These systems are very amenable to joining by FSW whereas the cutting of these materials is a significant processing contrast. They are extremely difficult to cut.

A perusal of the diversity of FSW systems, both same and dissimilar presented in this review provides a testament to the diversity of applications, particularly commercial, for FSW. The FSW of dissimilar, light-weight systems such as Al-alloys to Mg-alloys is encouraging for a host of aerospace and automotive applications (Ref 4, 5). The ability to computerize and automate the FSW process is conducive to integration into modularized manufacturing systems where dissimilar components can be joined without the distortions and complexities intrinsic to conventional fusion welding.

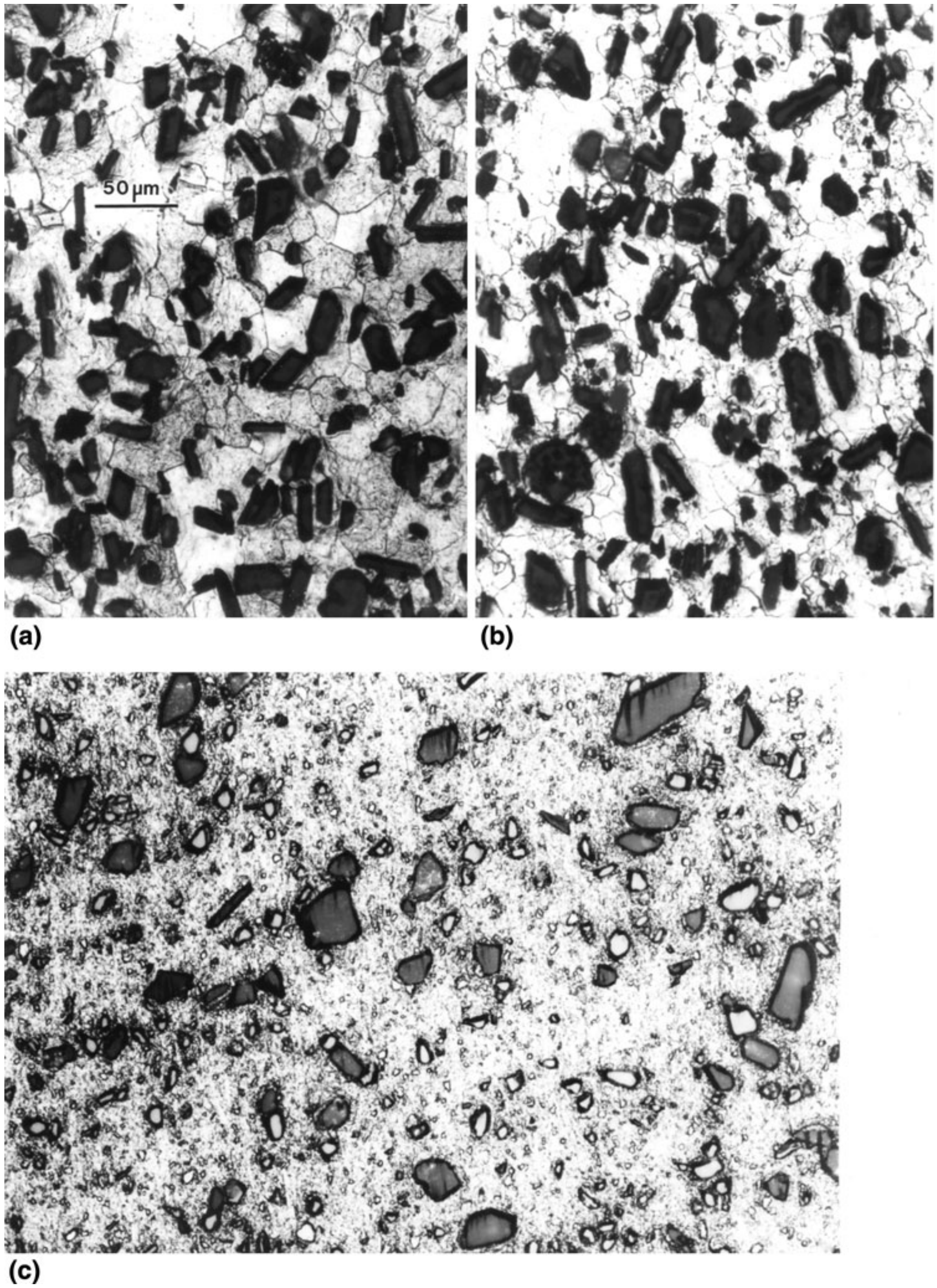

Fig. 19 Optical metallographic images comparing the Al 6061 + 20% Al_2O_3 base or work-piece microstructure (a) with the structure in the weld zone following FSW (b). (c) The mixing of Al_2O_3 base or work-piece microstructure (a)with the structure in the weld zone following FSW (b). (c) The mixing of Al_2O_3 and SiC particles in the weld zone for the FSW of Al 6061 + 20% Al_2O_3/A359 + 20% Al_2O_3

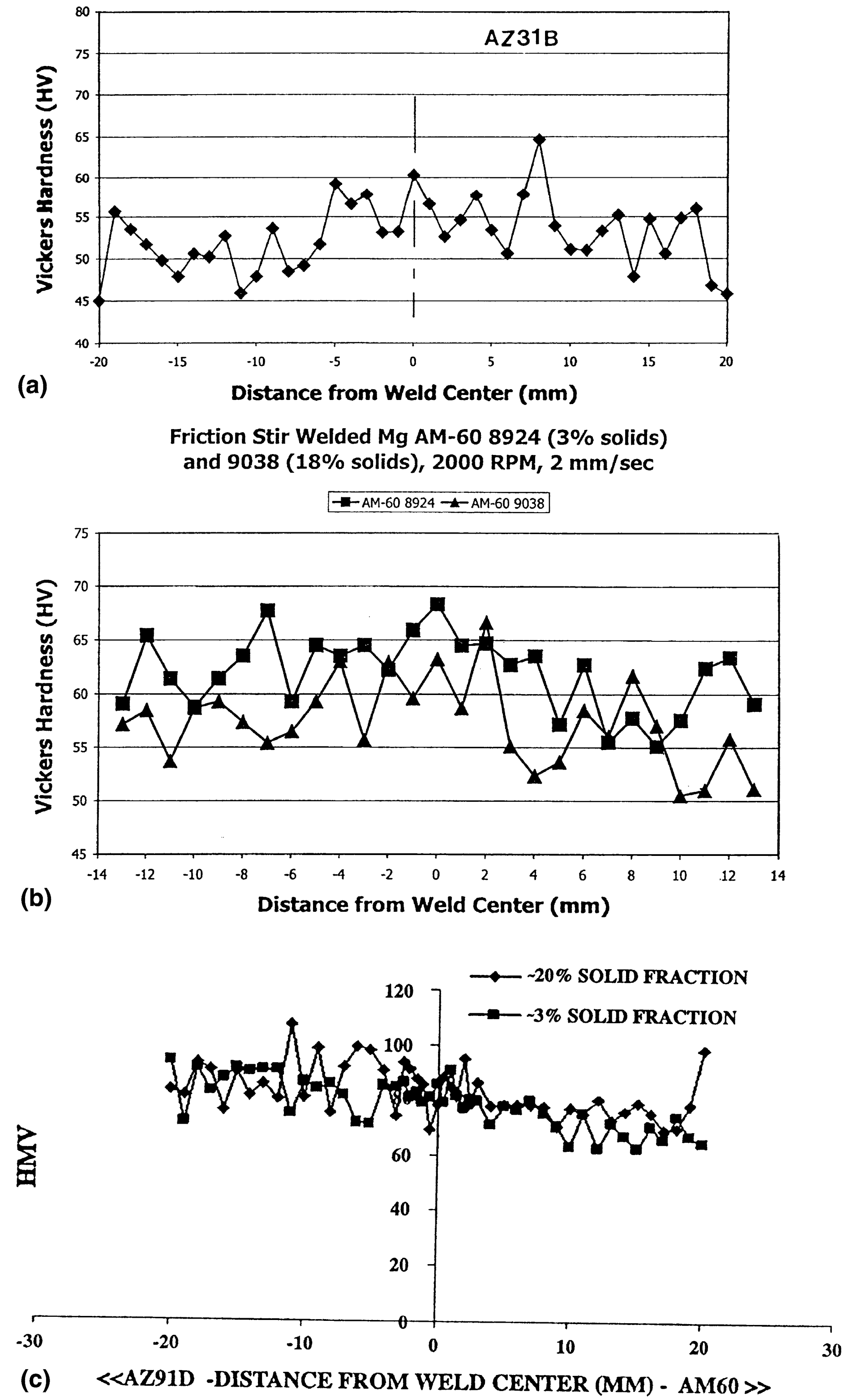

Fig. 20 Comparison of the weld zone/weld face residual hardness profiles for FSW of several magnesium alloy systems. (a) AZ31B (from Ref 29), (b) solid fractions of 3% and 18% AM60D (from Ref 28), (c) AZ91D/AM60D (3% and 20% solid fraction) (from Ref 33)

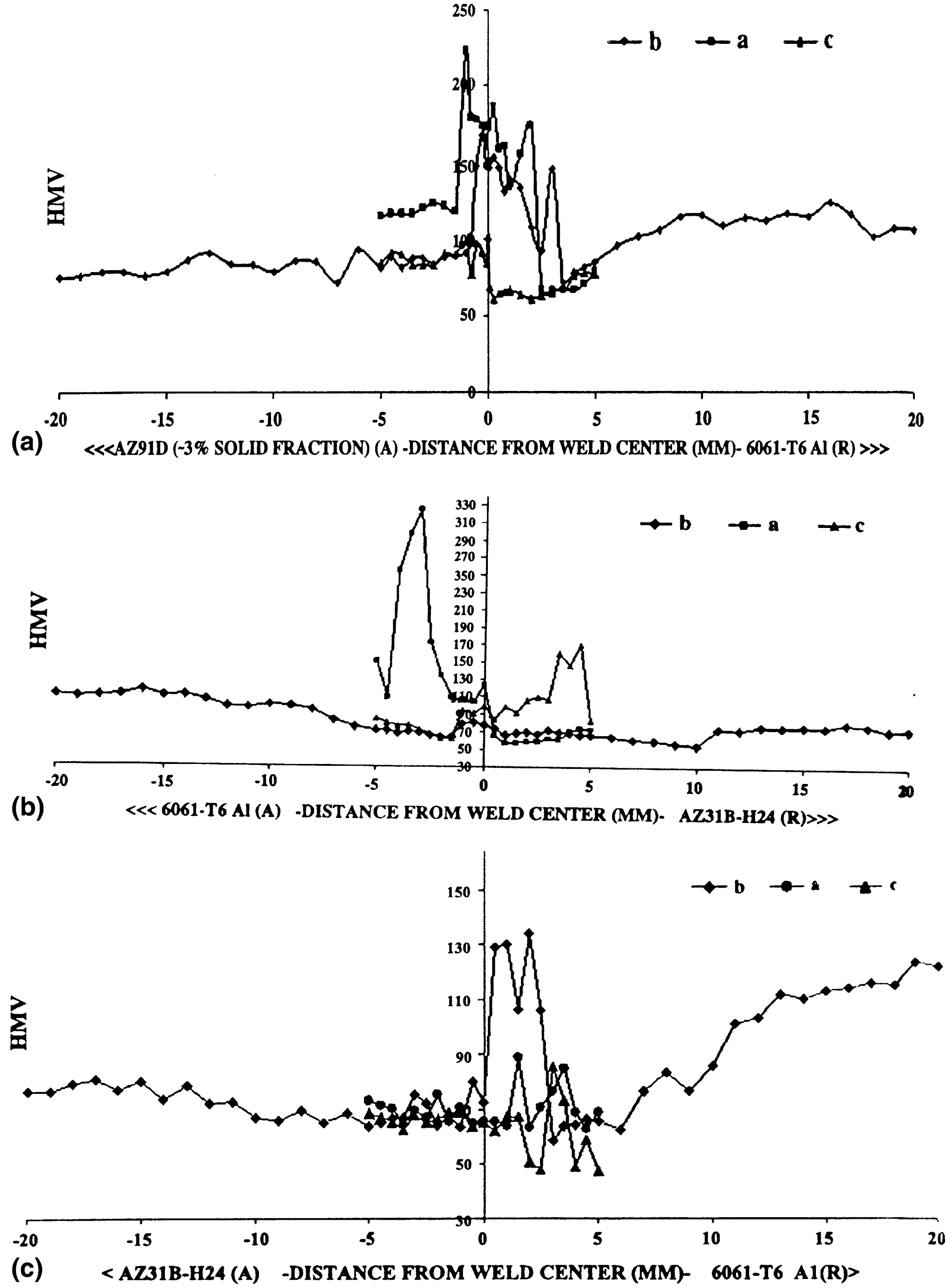

Fig. 21 Comparison of weld zone/weld face residual microindentation hardness profiles at different locations noted from the weld top-a, mid-section-b, and bottom-c: (a) AZ91D/Al 6061, (b) Al 6061/AZ31B, and (c) AZ31B/Al 6061; from Ref 33

Acknowledgments

This research was variously supported by NASA and DoD agencies over a period of more than 10 years (from 1996 to the present). Portions of this work were also supported over these years by a Mr. and Mrs. MacIntosh Murchison Chair at the University of Texas at El Paso.

References

1. I. Stol, Selecting Manufacturing Processes for Automotive Aluminum Space Frames, *Weld. J.*, 1994, **73**, p 57–65
2. R. Irving, Interest in Welded Aluminum Automobiles Gathers Momentum Worldwide, *Weld. J.*, 1998, **77**, p 31–35
3. M.R. Johnsen, Friction Stir Welding Takes off at Boeing, *Weld. J.*, 1999, **78**, p 35–39
4. P.F. Mendez and T.W. Eager, Welding Processes for Aeronautics, *Adv. Mater. Process.*, 2001, **159**, p 39–43
5. D. Burford, C. Widener, and B. Tweedy, Advances in Friction Stir Welding for Aerospace Applications, *Airframer*, 2007, **14**, p 3–7
6. G. Lütjering and J.C. Williams, *Titanium*, Springer, New York, 2007, p 109–113
7. D.G. Sanders, M. Ramulu, and P.D. Edwards, Superplastic Forming of Friction-Stir Welds in Titanium Alloy 6Al-4V: Preliminary Results, *Materialwissenshaft und We-kstofflechnik*, 2008, **39**, p 553–557
8. C. Meran, V. Kovan, and A. Alptekin, Friction Stir Welding of A101 304 Austenitic Stainless Steel, *Materialwissenschaff und We-kstoff-technik*, 2007, **38**(10), p 829–835

9. D.J. Shindo, A.R. Rivera, and L.E. Murr, Shape Optimization for Tool Wear in the Friction-Stir Welding of Cast Al 358-20% SiC, *J. Mater. Sci.*, 2002, **37**, p 4999–5005
10. R.A. Prado, L.E. Murr, K.F. Soto, and J.C. McClure, Self Optimization in Tool Wear for Friction-Stir Welding of Al 6061 + 20% Al_2O_3 MMC, *Mater. Sci. Eng.*, 2003, **A349**, p 156–165
11. M. Amirizad, A.H. Kokabi, M.A. Gharacheh, R. Sarrafi, B. Shalshi, and M. Azizieh, Evaluation of Microstructure and Mechanical Properties in Friction Stir Welded A356 + 15% SiC, Cast Composite, *Mater. Lett.*, 2006, **60**(4), p 565–568
12. C.G. Rhodes, M.W. Mahoney, W.H. Bingel, R.A. Spurling, and C.C. Bampton, Effects of Friction Stir Welding on Microstructure of 7075 Aluminum, *Scripta Mater.*, 1997, **36**, p 69–73
13. G. Liu, L.E. Murr, C.-S. Niou, J.C. McClure, and F.R. Vega, Microstructural Aspects of the Friction-Stir Welding of 6061-T6 Aluminum, *Scripta Mater.*, 1997, **37**, p 355–359
14. Y. Li, L.E. Murr, and J.C. McClure, Flow Visualization, Residual Microstructures Associated with the Friction-Stir Welding of 2024 Aluminum to 6061 Aluminum, *Mater. Sci. Eng.*, 1999, **A271**, p 213–223
15. S.H. Kazi and L.E. Murr, Complex Flow Phenomena Associated with Friction-Stir Welding of Aluminum Alloys, *Friction Stir Welding and Processing*, K.V. Jata, M.W. Mahoney, R.S. Mishra, S.L. Semiatin, and D.P. Field, Ed., 2001, The Minerals, Metals & Materials Soc., p 139–150
16. L.E. Murr, Y. Li, E.A. Trillo, and J.C. McClure, Fundamental Issues and Industrial Applications of Friction-Stir Welding, *Mater. Tech. Adv. Perform. Mater.*, 2000, **15**(1), p 37–48
17. L.E. Murr and C. Pizana, Dynamic Recrystallization: The Dynamic Deformation Regime, *Metall. Mater. Trans. A*, 2007, **38A**, p 2611–2628
18. L.E. Murr, G. Liu, and J.C. McClure, Dynamic Recrystallization in Friction-Stir Welding of 1100 Aluminum, *J. Mater. Sci. Lett.*, 1997, **16**, p 1801–1813
19. S. Benavides, Y. Li, L.E. Murr, D. Brown, and J.C. McClure, Low Temperature Friction-Stir Welding of 2024 Aluminum, *Scripta Mater.*, 1999, **41**(8), p 809–815
20. S. Benavides, Y. Li, and L.E. Murr, Ultrafine Grain Structure in the Friction-Stir Welding of Aluminum Alloy 2024 at Low Temperature, *Ultrafine Grained Materials*, R.S. Mishra, S.L. Semiatin, C. Suryanarayana, N.N. Thadhani, and T.C. Lowe, Ed., 2000, The Minerals, Metals and Materials Soc., p 155–163
21. F. Contreras, E.A. Trillo, and L.E. Murr, Friction-Stir Welding of Beryllium-Aluminum Powder Metallurgy Alloy, *J. Mater. Sci.*, 2001, **37**(1), p 89–99
22. L.E. Murr, E.A. Trillo, Y. Li, R.D. Flores, B.M. Nowak, and J.C. McClure, Solid-State Flow Associated with the Friction-Stir Welding of Dissimilar Metals, *Fluid Flow Phenomena in Metals Processing*, N. El-Kaddah, D.G.C. Robertson, S.T. Johansen, and V.R. Voller, Ed., The Minerals, Metals & Materials Society, 1999
23. W. Merzkirch, *Flow Visualization*, 2nd ed., Academic Press, Orlando, 1997
24. W. Tang, X. Guo, J.C. McClure, L.E. Murr, and A. Nunes, Heat Input and Temperature Distribution in Friction-Stir Welding, *J. Mater. Process. Manuf. Sci.*, 1998, **7**, p 163–172
25. L.E. Murr, Y. Li, E.A. Trillo, B.M. Nowak, and J.C. McClure, A Comparative Study of Friction-Stir Welding of Aluminum Alloys, *Aluminum Trans.*, 1999, **1**(1), p 141–154
26. L.E. Murr, G. Liu, and J.C. McClure, A TEM Study of Precipitation and Related Microstructures in the Friction-Stir Welded 6061 Aluminum, *J. Mater. Sci.*, 1998, **33**, p 1243–1251
27. L.E. Murr, G. Sharma, F. Contreras, M. Guerra, S.H. Kazi, M. Siddique, R.D. Flores, D.J. Shindo, K.F. Soto, E.A. Trillo, C. Schmidt, and J.C. McClure, Joining Dissimilar Aluminum Alloys and Other Metals and Alloys by Friction-Stir Welding, *Aluminum 2001—Proc. TMS 2001 Aluminum Automotive & Joining Sessions*, S.K. Das, J.G. Kaufman, and T.J. Lienert, Ed., The Minerals, Metals & Materials Soc., 2001
28. J.A. Esparza, W.C. Davis, and L.E. Murr, Microstructure-Property Studies in Friction-Stir Welded, Thixomolded Magnesium Alloy AM60, *J. Mater. Sci.*, 2003, **38**, p 941–952
29. J.A. Esparza, W.C. Davis, E.A. Trillo, and L.E. Murr, Friction-Stir Welding of Magnesium Alloy AZ31B, *J. Mater. Sci. Lett.*, 2002, **21**, p 917–920
30. A.C. Somasekharan and L.E. Murr, Characterization of Complex, Solid-State Flow and Mixing in the Friction-Stir Welding (FSW) of Aluminum Alloy 6061-T6 to Magnesium Alloy AZ91D Using Color Metallography, *J. Mater. Sci. Lett.*, 2006, **41**, p 5365–5370
31. R.D. Flores, L.E. Murr, D.J. Shindo, and E.A. Trillo, Friction-Stir Welding of Metals and Alloys: Fundamental Studies of Solid-State and Intercalated Flow, *J. Mater. Process. Technol.,* 2001, **117**(3), Sect. 1A
32. L.E. Murr, Y. Li, E.A. Trillo, R.D. Flores, and J.C. McClure, Microstructures in Friction-Stir Welded Metals, *J. Mater. Process. Manuf. Sci.*, 1998, **7**, p 146–161
33. A.C. Somasekharan and L.E. Murr, Microstructures in Friction-Stir Welded Dissimilar Magnesium Alloys and Magnesium Alloys to 6061-T6 Aluminum, *Mater. Character.*, 2004, **52**, p 49–64
34. A.C. Somasekharan and L.E. Murr, Fundamental Studies of the Friction-Stir Welding of Magnesium Alloys and Magnesium Alloys to 6061-T6 Aluminum, *Magnesium 2004*, A.A. Luo, Ed., The Minerals, Metals and Materials Society, Warrendale, PA, 2004, p 31-37
35. A.C. Somasekharan and L.E. Murr, Microstructural Details of Friction-Stir Weld Interfaces, *Friction Stir Welding and Processing III*, K.V. Jata, Ed., The Minerals, Metals and Materials Society, Warrendale, PA, 2005, p 261–267